Non-uniqueness, stability and bifurcation analyses in elasto-viscoplastic boundary value problems with no inertia

Huan Wang, Panagiotis Kotronis, Giulio Sciarra

Non-uniqueness, stability and bifurcation analyses in elasto-viscoplastic boundary value problems with no inertia

Huan WANG, Panagiotis KOTRONIS, Giulio SCIARRA

Ecole Centrale de Nantes, Université de Nantes, CNRS, Institut de Recherche en Génie Civil et Mécanique (GeM), UMR 6183, 1 rue de la Noë, BP 92101, Nantes, cedex 3, France

Abstract

The article focuses on non-uniqueness, bifurcation and stability conditions in elasto-viscoplastic boundary value problems when inertia terms are neglected. Analytical and numerical studies are presented to investigate the capability of an elasto-viscoplastic model to regularize the behavior in the occurrence of strain localization with respect to number of strain bands formed and mesh dependency. It is found that elasto-viscoplasticity in a Cauchy medium neither restores the uniqueness of the solution nor provides mesh independent results. A high value of the viscosity parameter can sometimes provide results that are mesh independent, up to a certain limit strain, as it actually modifies the response of the constitutive law by an ad-hoc increase of its hardening branch. On the contrary, coupling elasto-viscoplasticity with a second gradient model that introduces an internal length parameter reproduces realistically the rate dependent behavior and regularizes the results.

Keywords: Elasto-viscoplasticity, Uniqueness, Strain localization, Regularization, Second gradient, Bifurcation, Linear perturbation analysis, Stability

1. Introduction

It is well known that classical Cauchy continua do not have an internal length parameter and are therefore unable to reproduce strain localization, either diffuse or in the form of shear bands [1, 2, 3, 4]. To deal with this deficiency, different enhancements of classical continuum mechanics have been proposed; the non local integral approach in which an internal length is explicitly incorporated [2], models involving gradients of internal variables like plastic strain [1, 5, 6] or damage [7] which yield non local constitutive equations and media with microstructure, based on the pioneering work of Germain [8, 9] and Mindlin [10, 11] in which the internal length is indirectly introduced through a ratio of constitutive constants.

*Corresponding author

Viscoplasticity provides an elegant mathematical framework to reproduce the rate dependent non-linear material behavior [12, 13, 14, 15, 16, 17] and several studies focused on the use of viscoplastic models to regularize boundary value problems (see for example [18, 19, 20, 21, 22, 23, 24, 25, 26, 27, 28]). It is not the purpose of this paper to provide an extensive review of viscoplastic models and their thermodynamically consistent formulation. However, it is important to mention that the Perzyna, the Duvaut-Lions and the Consistency model, we are going to refer to in the following sections, can be inscribed into the general thermodynamically consistent framework proposed in the seminal works [29, 30, 31, 32, 33, 34, 35]. The reader interested to the subject is reported, for instance, to [36, 37, 38].

In the following, several results on the use of viscoplasticity to regularize boundary value problems are summarized:

- For dynamic problems (where inertia terms are considered), rate-dependency introduces a length-scale into the initial boundary value problem [39]. Using a linear perturbation analysis it has been shown that the growth rate of the perturbation becomes maximum for a zero wave length, but not infinite as in the case of rate-independent materials. As a consequence a finite characteristic time, corresponding to the time necessary for perturbations to propagate, and a characteristic length, given by the product of the elastic (shear) wave speed by the aforementioned characteristic time, can be introduced (see for instance [40]). Nevertheless, [41] recently showed assuming both the frequency and the wave number belonging to the complex plane that strain localization is possible for dynamic problems and the total strain and plastic strain rate profiles can exhibit a mesh dependent behavior.

- For transient problems (where inertia terms are neglected but the influence of time and of the loading rate are considered) the delaying role of viscosity in the appearance of strain localisation is illustrated for example in [22]. Nevertheless, mesh dependency still appears for important levels of deformation [22]. In [42, 43, 44] it is demonstrated that mesh dependency can also be encountered using damage models with rate effects. [45] states that for granular soils, when an elasto-viscoplastic strain softening model characterized by an experimental definition for the viscous nucleus is implemented, strain localization takes place and the numerical solution depends on mesh refinement. On the other hand [24] states that 'the inclusion of a damper in parallel to a plastic dissipative element seems to lead to a diffusion-type equation'.

- For quasi-static loading (where inertia terms and the influence of time and of the loading rate are negligible) a dispersion analysis cannot be carried out and therefore an internal length scale cannot be

determined [24]. It is stated however in [21] that 'numerical localization results for rate-independent solids can be interpreted as corresponding to solutions for the limit of vanishing rate dependence for a solid with an imperfection, of whatever origin, that induces a shear band one element wide. Provided that the element size is such that this shear band width is appropriate for the particular situation being modelled, the numerically obtained solution is a pertinent one'.

It is therefore apparent that a conclusive clarification of expected results of elasto-viscoplastic constitutive models is required in terms of uniqueness and stability of the solution of the boundary value problem as well as of the solution mesh-dependency when this last is obtained numerically. The purpose of the present article is to investigate non-uniqueness, bifurcation and stability conditions for the case of elasto-viscoplastic transient boundary value problems (where, as stated before, inertia terms are neglected but the influence of time and of the loading rate are considered), in order to have a better insight on the viscous type regularization efficiency. Some conclusions for the quasi-static case are also given at the end of the paper.

The article is organized as follows: section 2 recalls the formulation of the elasto-viscoplastic constitutive models used in the present paper, the conditions for the loss of uniqueness of the solution of the boundary problem and an algorithm of random initialization to identify the different possible bifurcated solutions. Sections 3 and 4 present analytical and numerical studies in a classical (Cauchy) medium to verify the capability of the elasto-viscoplastic model to cure the degenerated behavior in the occurrence of strain localization with respect to mesh dependency and number of bands formed for the case of elasto-viscoplastic transient boundary value problems. Finally, the same analysis is carried out in sections 5 and 6 where analytical and numerical studies are presented for a second gradient elasto-viscoplastic medium. Section 7 summarizes the main results and findings.

The following notations are adopted; compression is positive, tensor indices are located at the lower position, bold non italic letters are used for vectors, bold italic letters for matrices/tensors, $\mathbf{0}$ is the zero vector or zero second order tensor. Dots denote derivatives with respect to time and the superscript ^{T} the transpose. The study is conducted using the small strain hypothesis and inertia forces as well as body forces are neglected. All calculations are done using a finite element code based on Matlab, initially developed by [46]. GMSH [47] is used for the mesh generator and post processing of the results.

2. Materials and methods

2.1. Viscoplastic models

Three families of viscoplastic constitutive models are often cited in the literature, the Perzyna [12, 13], the Duvaut-Lions [14] and the Consistency model [25, 26]. The two former are known as overstress models due to the fact that the stress state can stay outside the yield surface. Furthermore, the plastic strain is explicitly defined in overstress models. On the contrary, the viscoplastic consistency model does not allow the stress state to be outside the yield surface, i.e. the consistency condition of classical plasticity is satisfied [26]. In the consistency model the yield function depends not only on the stress and hardening variables but also on their time derivatives. Therefore, strain rate affects the evolution of the yield surface (hardening, softening, size, shape).

In small strain viscoplasticity, the following additive decomposition of total strain ε is considered:

$$\dot{\varepsilon} = \dot{\varepsilon}^e + \dot{\varepsilon}^{vp} \tag{1}$$

where $\dot{\varepsilon}^e$ denotes the elastic strain rate, $\dot{\varepsilon}^{vp}$ the viscoplastic strain rate and the superscript $\dot{(\cdot)}$ the derivative with respect to time.

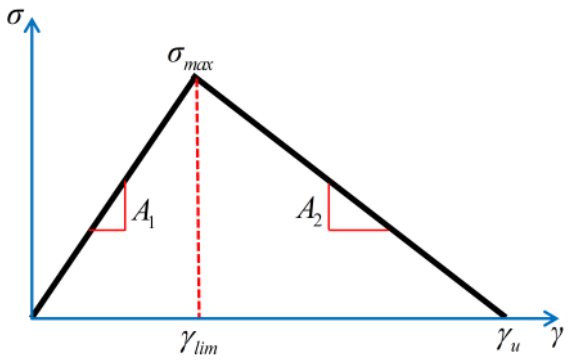

Figure 1: Piecewise constitutive law

The yield surface of the Consistency viscoplastic model depends on the strain and the strain rate. For the 1D case (see Fig 1) one gets:

$$f(\sigma, \gamma, \dot{\gamma}) = \sigma - \sigma_{max} - \gamma^{vp} \frac{A_1 A_2}{A_2 - A_1} - y\dot{\gamma}^{vp} \tag{2}$$

where y the hardening function related to the strain rate effect (see Appendix A).

It is shown in [25] and in the Appendix A. that with an appropriate choice of the model parameters, the 1D viscoplastic strain rates of the three families of viscoplastic constitutive models become identical. If for example the rate independent part has the form presented in Fig. 1, the 1D viscoplastic strain rate $\dot{\gamma}^{vp}$ for the three models can be set equal to:

$$\dot{\gamma}^{vp} = \frac{1}{\eta\sigma_{max}}[\sigma - \sigma_{max} - A_2(\gamma - \gamma_{lim})] \tag{3}$$

with A_1 the modulus of the elastic part, A_2 the modulus of the softening part, η the viscosity, σ_{max} the yield stress, γ_{lim} the corresponding strain and γ_u the ultimate strain, see Fig. 1. Equation (3) is adopted hereafter, so that the results of the one-dimensional analysis presented in section 3 are valid for the three families of viscoplastic constitutive models. The main equations of the 1D elasto-viscoplastic model are finally provided in Table 1.

Additive decomposition of total strain	$\dot{\varepsilon} = \dot{\varepsilon}^e + \dot{\varepsilon}^{vp}$
Yield surface	$f(\sigma, \gamma, \dot{\gamma}) = \sigma - \sigma_{max} - \gamma^{vp}\frac{A_1 A_2}{A_2 - A_1} - y\dot{\gamma}^{vp}$
Hardening function	$y = \eta\sigma_{max}$
Viscoplastic strain rate	$\dot{\gamma}^{vp} = \frac{1}{\eta\sigma_{max}}[\sigma - \sigma_{max} - A_2(\gamma - \gamma_{lim})]$

Table 1: The 1D elasto-viscoplastic model

2.2. Uniqueness & bifurcation

In this section we reorganize information available in the literature, following in particular [48] and [49, Chapter 11]. According to the classical argument adopted by Kirchoff to prove the uniqueness theorem in the framework of small strain elasticity, a sufficient condition for uniqueness of the non-linear (visco-) plastic problem is provided by the second-order work (Hill's criterion):

$$\int_V \Delta\dot{\boldsymbol{\sigma}} : \Delta\dot{\boldsymbol{\varepsilon}}\, dV > 0 \tag{4}$$

where V is the body volume, $\Delta\dot{\boldsymbol{\sigma}}$ satisfies equilibrium and homogeneous traction boundary conditions on the part of the boundary where natural boundary conditions are prescribed, while $\Delta\dot{\boldsymbol{\varepsilon}}$ verifies homogeneous conditions on the part of the boundary where essential boundary conditions are given. According to Hill's comparison theorem (see e.g. [48]) a sufficient condition for uniqueness is

$$\int_V \dot{\boldsymbol{\sigma}} : \dot{\boldsymbol{\varepsilon}}\, dV > 0 \tag{5}$$

for all kinematically admissible velocity fields, which can be localized into

$$\dot{\boldsymbol{\sigma}} : \dot{\boldsymbol{\varepsilon}} > 0. \tag{6}$$

This last condition is called positiveness of the local second-order work. When an incrementally linear formulation of the constitutive equations exists, say when the consistent tangent four-rank tensor $\boldsymbol{C}$ can be defined, as in the case of rate independent plasticity or of the Consistency viscoplastic model, the positiveness of the local second-order work is equivalent to the definite positiveness of the symmetric part of $\boldsymbol{C}$.

Starting from equation (6), exclusion of bifurcation fails to hold when the positive definiteness of the constitutive operator $\boldsymbol{C}$ is lost, that is when at least one tensor $\mathbf{X} \neq \mathbf{0}$ exists such that:

$$\mathbf{X} \cdot \boldsymbol{C}[\mathbf{X}] = \mathbf{0} \tag{7}$$

where $\boldsymbol{C}[\mathbf{X}]$ is a the second order tensor whose ij component is $\boldsymbol{C}_{ijkl}\mathbf{X}_{kl}$.

Equation (7) does not mean that $\boldsymbol{C}$ is necessarily singular as in the general case of non-associative plasticity one can verify Eq (7) even if $\boldsymbol{C}[\mathbf{X}] \neq \mathbf{0}$. Therefore, loss of positive definiteness does not necessarily imply bifurcation. Conversely the non singularity condition of the constitutive operator $\boldsymbol{C}$ can be written as:

$$\boldsymbol{C}[\mathbf{X}] \neq \mathbf{0} \tag{8}$$

for every tensor $\mathbf{X} \neq \mathbf{0}$, see again [49]. It is clear that failing to satisfy (8) is critical for the bifurcation of the homogeneous solution. Consider now the so called (semi-) strong ellipticity conditions for the constitutive operator $\boldsymbol{C}$, say

$$\mathbf{g} \cdot \boldsymbol{C}[\mathbf{g} \otimes \mathbf{n}]\mathbf{n} \geq 0, \forall \mathbf{n} \in V, \quad \|\mathbf{n}\| = 1 \quad \text{and} \quad \mathbf{g} \neq \mathbf{0} \tag{9}$$

which may be expressed, in a different notation, as the positive (semi-)definiteness of the acoustic tensor $\boldsymbol{A}(\mathbf{n})$

$$\mathbf{g} \cdot \boldsymbol{A}(\mathbf{n})\mathbf{g} = \mathbf{g} \cdot \boldsymbol{C}[\mathbf{g} \otimes \mathbf{n}]\mathbf{n} \geq 0 \tag{10}$$

It is possible to prove [50] that when the inequality (10) is not satisfied during a loading program of a generic boundary value problem, the sufficient condition (4) does not hold true. As in the previous discussion about the constitutive operator $\boldsymbol{C}$, when condition (10) fails the acoustic tensor can still be non-singular. A similar non singularity condition as that of equation (8) for the constitutive operator can be introduced for

the acoustic tensor, the so-called ellipticity condition (Rice criterion):

$$det\boldsymbol{A}(\mathbf{n}) \neq 0, \forall \mathbf{n} \in V, \|\mathbf{n}\| = 1 \tag{11}$$

It is also possible to prove that failure of ellipticity describes a shear band formation, i.e. strain localization into a planar band, as depicted in Fig 2 [51]. In plane strain case, the direction normal to the shear band can be expressed as

$$\mathbf{n} = \begin{bmatrix} \sin\theta \\ \cos\theta \end{bmatrix} \tag{12}$$

where θ is prescribed to be the angle between $\mathbf{n}$ and x-axis and let $z = \tan\theta$. Then the determinant of the acoustic tensor becomes according to Ortiz [52]:

$$\det(\boldsymbol{A}) = a_4 z^4 + a_3 z^3 + a_2 z^2 + a_1 z^1 + a_0 \tag{13}$$

with a_0, a_1, a_2, a_3, a_4 defined in terms of the constitutive tangent moduli:

$$\begin{aligned}
a_0 &= \boldsymbol{C}_{1111}\boldsymbol{C}_{1212} - \boldsymbol{C}_{1112}\boldsymbol{C}_{1211} \\
a_1 &= \boldsymbol{C}_{1111}\boldsymbol{C}_{1222} + \boldsymbol{C}_{1111}\boldsymbol{C}_{2212} - \boldsymbol{C}_{1112}\boldsymbol{C}_{2211} - \boldsymbol{C}_{1122}\boldsymbol{C}_{1211} \\
a_2 &= \boldsymbol{C}_{1111}\boldsymbol{C}_{2222} + \boldsymbol{C}_{1112}\boldsymbol{C}_{1222} + \boldsymbol{C}_{1211}\boldsymbol{C}_{2212} - \boldsymbol{C}_{1122}\boldsymbol{C}_{1212} - \boldsymbol{C}_{1122}\boldsymbol{C}_{2211} - \boldsymbol{C}_{1212}\boldsymbol{C}_{2211} \\
a_3 &= \boldsymbol{C}_{1112}\boldsymbol{C}_{2222} + \boldsymbol{C}_{1211}\boldsymbol{C}_{2222} - \boldsymbol{C}_{1122}\boldsymbol{C}_{2212} - \boldsymbol{C}_{1222}\boldsymbol{C}_{2211} \\
a_4 &= \boldsymbol{C}_{1212}\boldsymbol{C}_{2222} - \boldsymbol{C}_{2212}\boldsymbol{C}_{1222}
\end{aligned} \tag{14}$$

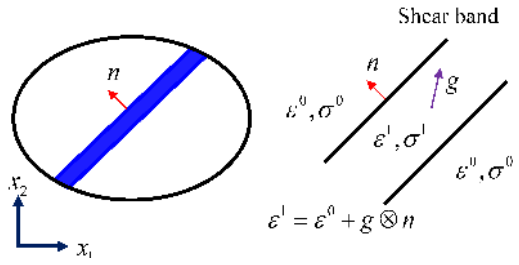

Figure 2: Principle scheme of a shear band

Following for instance Bigoni [49] we can summarize the previous remarks as follows:

- the positive definiteness of the constitutive operator $\boldsymbol{C}$ implies the non singularity, as well as the non singularity condition (ellipticity condition) of the acoustic tensor, equation (11).

- the opposite is in general not true; the loss of uniqueness, characterized by violating the non-singularity condition of the constitutive operator $\boldsymbol{C}$ does not necessarily imply violation of the ellipticity condition of the acoustic tensor. From the physical point of view different bifurcated solutions can arise before the occurrence of shear band.

It is important to notice at this point that the overstress models of the Perzyna and Duvaut-Lions type (see section 2.1) do not enable the definition of a tangent stiffness operator.

2.3. Algorithm for finding bifurcations of the homogeneous solution (random initialization)

For a finite element discretization of the boundary value problem, Hill's criterion (5) reads as:

$$\int_V \dot{\mathbf{u}}^T \boldsymbol{B}^T \boldsymbol{C}\, \boldsymbol{B}\, \dot{\mathbf{u}}\, dV = \dot{\mathbf{u}}^T \boldsymbol{K}\, \dot{\mathbf{u}} > 0 \tag{15}$$

where $\boldsymbol{K} = \boldsymbol{B}^T\, \boldsymbol{C}\, \boldsymbol{B}$ is the global stiffness matrix, $\boldsymbol{B}$ a matrix function of the finite element shape functions and $\dot{\mathbf{u}}$ the vector of nodal velocities. Note that the boundary conditions at the beginning of section 2.2 must hold true. The sufficient condition (5) can be therefore rephrased by :

$$\dot{\mathbf{u}}^T \boldsymbol{K}\, \dot{\mathbf{u}} > 0 \tag{16}$$

According to Vieta's rule, equation (16) turns into

$$det(\boldsymbol{K}) = \prod_{i=1}^{n} \omega_i > 0 \tag{17}$$

with ω_i the i-th eigenvalue of $\boldsymbol{K}$. If we restrict our attention to the non sigularity condition (8), we can state that bifurcation of the homogeneous solution emerges when the minimum eigenvalue of the global stiffness matrix $\boldsymbol{K}$ vanishes.

As already pointed out by [53], a zero eigenvalue is hard to get due to numerical round-off errors. Perturbation techniques can be therefore used while the minimum eigenvalue is (slightly) negative to check the existence of multiple solutions (see for example [54] for a random initialization of the Newton-Raphson scheme).

As proposed in [53], having determined the bifurcation point by an eigenvalue analysis of the tangent stiffness matrix, continuation of the localization branch instead of the fundamental branch can be forced by

adding a part of the eigenmode which belongs to the vanishing eigenvalue to the incremental displacement field of the fundamental part as follows:

$$\Delta\mathbf{a} = \alpha(\Delta\mathbf{a}^f + \beta\mathbf{v}_1) \tag{18}$$

where $\Delta\mathbf{a}$ is the trial displacement increment of the bifurcated solution, $\mathbf{v}_1$ is the eigenvector corresponding to the vanishing eigenvalue and $\Delta\mathbf{a}^f$ is the displacement increment of the fundamental path. α and β scalars can be found considering different assumptions, the ones made by de Borst [53] are adopted hereafter.

The first assumption is that the trial displacement increment is orthogonal to the fundamental path and therefore:

$$(\Delta\mathbf{a})^{\mathrm{T}}\Delta\mathbf{a}^f = 0 \tag{19}$$

By introducing equation (18) into equation (19) β is found:

$$\beta = -\frac{(\Delta\mathbf{a}^f)^{\mathrm{T}}\Delta\mathbf{a}^f}{(\Delta\mathbf{a}^f)^{\mathrm{T}}\mathbf{v}_1} \tag{20}$$

The trial displacement increment of the bifurcated solution turns therefore into:

$$\Delta\mathbf{a} = \alpha\{\Delta\mathbf{a}^f - \frac{(\Delta\mathbf{a}^f)^{\mathrm{T}}\Delta\mathbf{a}^f}{(\Delta\mathbf{a}^f)^{\mathrm{T}}\mathbf{v}_1}\mathbf{v}_1\} \tag{21}$$

However, as stated in [53], equation (21) fails when the bifurcation mode is orthogonal to the fundamental path ($(\Delta\mathbf{a}^f)^{\mathrm{T}}\mathbf{v}_1 = 0$). A remedy is to normalize $\Delta\mathbf{a}$ such as

$$(\Delta\mathbf{a}^f)^{\mathrm{T}}\Delta\mathbf{a}^f = (\Delta\mathbf{a})^{\mathrm{T}}\Delta\mathbf{a} \tag{22}$$

The second assumption considers therefore that the norm of the displacement increment of the fundamental path and the norm of the trial displacement increment of the bifurcated solution are the same. The trial displacement increment of the bifurcated solution becomes:

$$\Delta\mathbf{a} = \frac{1}{\sqrt{(\Delta\mathbf{a}^f)^{\mathrm{T}}\Delta\mathbf{a}^f - [\Delta\mathbf{a}^f)^{\mathrm{T}}\mathbf{v}_1]^2}}\{(\Delta\mathbf{a}^f)^{\mathrm{T}}\mathbf{v}_1\Delta\mathbf{a}^f - (\Delta\mathbf{a}^f)^{\mathrm{T}}\Delta\mathbf{a}^f\mathbf{v}_1\} \tag{23}$$

The denominator of equation 23 now never vanishes, since this would imply that the eigenmode is identical with the fundamental path [53, 55].

Other ways to determine the scalar parameters α and β can be found in [56, 57].

Depending on the chosen perturbation, numerical calculations can diverge or converge to a new solution or to the fundamental solution [58]. The procedure can be summarized as follows:

1. Choose a step in the global response curve to study if there are multiple solutions (in addition to the fundamental one).
2. Use equation (23) to find the bifurcated solution.
3. Run the calculations to check if the code converges.
4. If convergence, continue the calculations to illustrate the evolution of the response for the remaining time steps.

In the following, analytical and numerical studies in a classical (sections 3 and 4) and in a second gradient medium (sections 5 and 6) are presented.

3. One-dimensional analytical and numerical study in a Cauchy medium

Consider a 1D bar subjected to an axial displacement at the right end and fixed at the left, see Fig 3. The boundary conditions are:

$$\begin{aligned} u(0) &= 0 \\ u(L) &= Vt \end{aligned} \tag{24}$$

where $V = \frac{\partial u(L)}{\partial t}$ indicates the loading rate, $u(0)$ and $u(L)$ the displacements at the two extremities and L the bar length. Without loss of generality a piecewise linear constitutive law is adopted Fig 1, where $A_1 > 0$

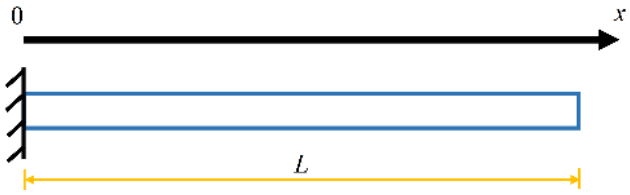

Figure 3: 1D bar

and $A_2 < 0$ specify respectively the positive and negative slope and γ_{lim} the limit strain at the stress peak (see also [59]). In the absence of viscous terms, the rate independent yield function f is given by

$$f(\sigma,\gamma) = \begin{cases} \sigma - \sigma_{max} & (\gamma < \gamma_{lim}) \\ \sigma - \sigma_{max} - A_2(\gamma - \gamma_{lim}) & (\gamma_{lim} < \gamma < \gamma_u) \end{cases} \tag{25}$$

where $f(\sigma_{max}, \gamma_{lim}) = f(0, \gamma_u) = 0$.

In order to study the behavior of the three viscoplastic models (the Perzyna, the Duvaut-Lions and the

Consistent model) the 1D viscoplastic strain rate is chosen equal to (see section 2.1 and [25]):

$$\dot{\gamma}^{vp} = \frac{1}{\eta\sigma_{max}}[\sigma - \sigma_{max} - A_2(\gamma - \gamma_{lim})] \tag{26}$$

In the following, we first investigate the loss of uniqueness of the solution for the 1D viscoplastic boundary value problem with no inertia (section 3.1) and then we perform a linear stability analysis (section 3.2).

3.1. Loss of uniqueness

The stress-strain relation of the viscoplastic 1D problem is:

$$\dot{\sigma} = A_1(\dot{\gamma} - \dot{\gamma}^{vp}) \tag{27}$$

A constant loading velocity V applied at the right end of the beam (equation (24)) results in a constant strain rate given by:

$$\dot{\gamma} = V/L \tag{28}$$

Introducing the viscoplastic strain equation (26) into equation (27) provides:

$$\dot{\sigma} = A_1\{\dot{\gamma} - \frac{1}{\eta\sigma_{max}}[\sigma - \sigma_{max} - A_2(\gamma - \gamma_{lim})]\} \tag{29}$$

After some rearrangements, the governing equation of the problem is finally given by the following first order linear differential equation:

$$\dot{\sigma} = -\frac{A_1}{\eta\sigma_{max}}\sigma + A_1\dot{\gamma} + \frac{A_1}{\eta} + \frac{A_1A_2}{\eta\sigma_{max}}(\gamma - \gamma_{lim}) \tag{30}$$

If we assume the initial state corresponding to the peak of the rate-independent constitutive law, so that $\sigma\,|_{t=0} = \sigma_{max}$ and $\gamma\,|_{t=0} = \gamma_{lim}$, the solution of equation (30) is found:

$$\sigma\,(t) = C_1 \mathrm{e}^{-\frac{A_1 t}{\eta\,\sigma_{max}}} - \frac{\dot{\gamma}\sigma_{max}\eta A_2}{A_1} + A_2\dot{\gamma}t + \dot{\gamma}\sigma_{max}\eta + \sigma_{max} \tag{31}$$

with C_1 a constant determined from the initial condition $\sigma\,|_{t=0} = \sigma_{max}$ as:

$$C_1 = \frac{\dot{\gamma}\sigma_{max}\eta A_2}{A_1} - \dot{\gamma}\sigma_{max}\eta \tag{32}$$

The stress is therefore expressed as:

$$\sigma(t) = [\frac{\dot{\gamma}\sigma_{max}\eta A_2}{A_1} - \dot{\gamma}\sigma_{max}\eta]e^{-\frac{A_1 t}{\eta\,\sigma_{max}}} - \frac{\dot{\gamma}\sigma_{max}\eta A_2}{A_1} + A_2\dot{\gamma}t + \dot{\gamma}\sigma_{max}\eta + \sigma_{max} \tag{33}$$

Numerical examples of the 1D bar problem are shown in Fig 4 considering different loading rates and the following parameters: $A_1 = 150kPa, A_2 = -75kPa, \gamma_{lim} = 0.1, \eta = 50kPa \cdot s$, $v_1 = 0.01m/s, v_2 = 0.005m/s, v_3 = 0.001m/s, v_4 = 0m/s$ (rate-independent).

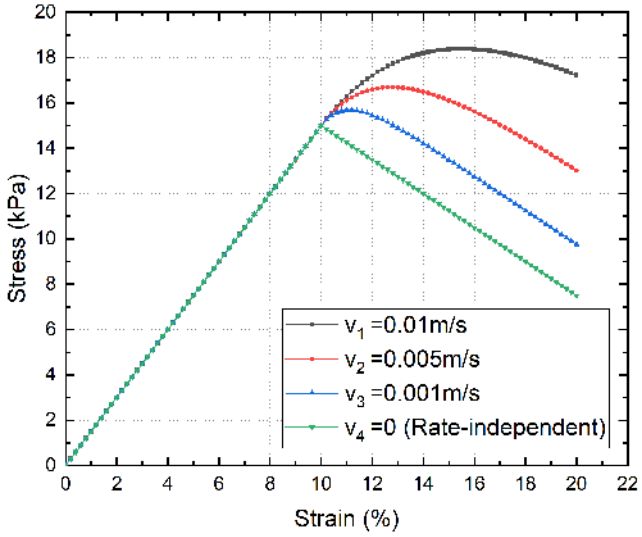

Figure 4: Stress-strain behaviour in the 1D bar considering different strain velocities

It can be clearly seen that depending on the chosen loading rate the peak points of the rate-dependent curves are not the same and therefore the positive definiteness of the second order work is expected to be lost at different strain levels, as it will be clearly illustrated in the following section.

3.1.1. Hill's criterion

The loss of uniqueness is first studied hereafter using Hill's criterion. The expression for $\Delta\dot{\sigma}$ in terms of $\Delta\dot{\gamma}$ can be deduced by differentiating equation (33), as this last does not explicitly account for the imposed displacement boundary condition. The second order work is found:

$$\Delta\dot{\gamma}\Delta\dot{\sigma} = \Delta\dot{\gamma}^2 e^{-\frac{A_1 t}{\eta\sigma_{max}}}(A_2 e^{\frac{A_1 t}{\eta\sigma_{max}}} + A_1 - A_2) \tag{34}$$

A critical time t_c therefore exists such that for $t \geq t_c$ the positive definiteness of the second order work is lost:

$$t_c = \frac{\eta\sigma_{max}}{A_1} \ln\left(\frac{A_2 - A_1}{A_2}\right) \tag{35}$$

The terms $\Delta\dot{\gamma}^2 e^{-\frac{A_1 t}{\eta\,\sigma_{max}}}$ and $(A_2 e^{\frac{A_1 t}{\eta\,\sigma_{max}}} + A_1 - A_2)$ are both positive initially after the peak point of the rate-independent solution. With increasing time, the slope of the rate-dependent curves decreases and for $t > t_c$ it becomes negative (as the term $(A_2 e^{\frac{A_1 t}{\eta\,\sigma_{max}}} + A_1 - A_2)$ becomes negative). Hill's criterion in the form of equation (4) being a sufficient condition for uniqueness, a bifurcation point can thus appear for $t \geq t_c$. At t_c, the critical strain γ_c corresponds to the peak stress value and it is found equal to:

$$\gamma_c = \gamma_{lim} + \dot{\gamma} t_c = \gamma_{lim} + \frac{\dot{V}}{L} t_c = \gamma_{lim} + \frac{\dot{V}\eta\sigma_{max}}{A_1 L} \ln\left(\frac{A_2 - A_1}{A_2}\right) \tag{36}$$

3.1.2. Acoustic tensor

As discussed in section 2.2, a particular form of loss of uniqueness is the formation of a shear band, occurring when the determinant of the acoustic tensor vanishes (see equation (11), n being the outward normal unit vector to the localization band, which in the 1D case coincides with the direction of the bar). The tangent modulus $\mathbf{C}$ is in this case a scalar and it can easily be obtained as:

$$C = \frac{\dot{\sigma}}{\dot{\gamma}} = e^{-\frac{A_1 t}{\eta\,\sigma_{max}}} (A_2 e^{\frac{A_1 t}{\eta\,\sigma_{max}}} + A_1 - A_2) \tag{37}$$

The determinant of the acoustic tensor $A(n)$ is therefore

$$det(A) = e^{-\frac{A_1 t}{\eta\,\sigma_{max}}} (A_2 e^{\frac{A_1 t}{\eta\,\sigma_{max}}} + A_1 - A_2) \tag{38}$$

indicating that $det(A) = 0$ holds true at same critical time t_c when Hill's criterion in the form of equation (4) fails, i.e. the peak point of the stress-stain curve.

3.1.3. Bifurcated solutions

The existence of multiple bifurcated solutions when using viscoplastic models is addressed hereafter. Following the illustration presented in [59] for rate independent models, let us assume a localized solution so that one part of the bar unloads elastically (hard part) and the other softens (soft part), see Fig 5. The characteristic size of the localized solution in what follows is termed l.

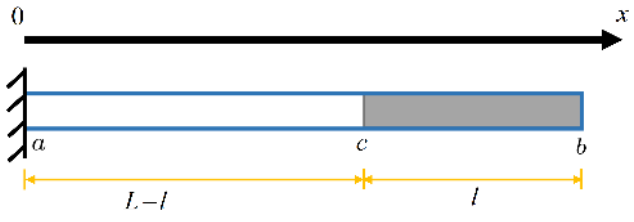

Figure 5: 1D bar; a hard (white) - soft (grey) localized solution

We denote hereafter the quantities inside the soft band by a superscript "1" and the quantities outside the band by a superscript "0". Equilibrium condition requires continuity of stresses; moreover, the longitudinal displacements should also be continuous. This implies that at the junction c one has:

$$\begin{aligned} u^0 &= u^1 = u^c \\ \sigma^0 &= \sigma^1 = \sigma^c \end{aligned} \tag{39}$$

The strain rate is assumed uniformly distributed in both parts of the bar with a jump across the band. Compatibility equations set the relationship between the strain rates:

$$\begin{aligned} \int_a^c \dot{\gamma}^0 \, dx &= \dot{u}^c - \dot{u}^a = \dot{u}^c \\ \int_c^b \dot{\gamma}^1 \, dx &= \dot{u}^b - \dot{u}^c = V - \dot{u}^c \end{aligned} \tag{40}$$

The integration of equations (40) leads to

$$\dot{\gamma}^0 = \frac{V - \dot{\gamma}^1 l}{L - l} \tag{41}$$

Outside the band the behavior is elastic and thus the stress-strain rate relation gives

$$\dot{\sigma}^0 = A_1 \dot{\gamma}^0 \tag{42}$$

Inside the band, the bar is submitted to a viscoplastic loading and the stress rate is given by equation (29):

$$\dot{\sigma}^1 = A_1 \{ \dot{\gamma}^1 - \frac{1}{\eta \sigma_{max}} [\sigma - \sigma_{max} - A_2(\gamma - \gamma_{lim})] \} \tag{43}$$

Combining equation (42) and equation (43) and considering a continuous stress state, the two unknown strain rates are given as:

$$A_1 \{ \dot{\gamma}^1 - \frac{1}{\eta \sigma_{max}} [\sigma - \sigma_{max} - A_2(\gamma - \gamma_{lim})] \} = A_1 \dot{\gamma}^0 \tag{44}$$

Equations (41) and (44) constitute a linear algebraic system of equations whose solution are the strain rates:

$$\begin{aligned} \dot{\gamma}^0 &= \frac{\eta \sigma_{max} V - [\sigma - \sigma_{max} - A_2(\gamma - \gamma_{lim})] l}{\eta \sigma_{max} L} \\ \dot{\gamma}^1 &= \frac{(L - l) \left[\sigma - \sigma_{max} - A_2(\gamma - \gamma_{lim}) \right] + \eta \sigma_{max} V}{\eta \sigma_{max} L} \end{aligned} \tag{45}$$

A viscoplastic constitutive law as the one studied in this paper does not allow to introduce any internal length parameter. An infinite number of localized solutions is therefore possible, depending on the value of

l. The two extreme solutions are found for $l = 0$ and $l = L$. The solution for $l = 0$ corresponds to stain localization inside a zero length zone and therefore to a spurious dissipation indicating mesh dependency (see also section 4.3.2). The solution for $l = L$ is the homogeneous solution. All the other intermediate solutions are possible. Fig 5 is an example of a typical localized pattern. Other patterns corresponding to alternative spatial distributions of soft and hard zones are however possible, as long as the total size of the soft parts is equal to l. Fig 6 for example illustrates two other patterns, a hard-soft-hard and a soft-hard-soft solution. The above conclusions are similar to the ones obtained for rate-independent constitutive laws that do not have any internal length parameter [59].

Another way to illustrate the different possible solutions is to use the random initialization technique

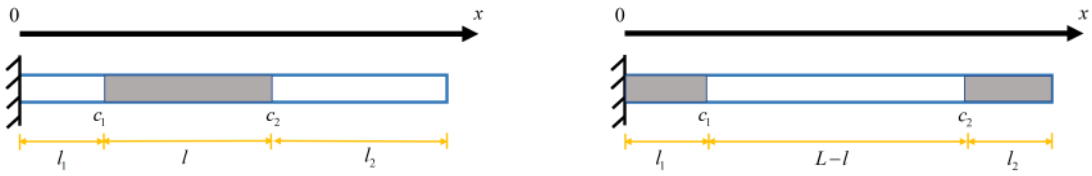

(a) Possible solution of hard-soft-hard form

(b) Possible solution of soft-hard-soft form

Figure 6: A hard-soft-hard (a) and a soft-hard-soft solution (b) of equation (45)

(section 2.3). Three typical converged solutions are presented in Fig 7 for a given loading rate V, where a random initialisation was applied at the peak (the point where the Hill's criterion is no longer satisfied). Near the peak, the three solutions seem similar to the homogeneous solution when looking at the global level, Fig 7. The local results (distribution of the accumulated equivalent plastic strain) however show differences and different localization patterns, Fig. 8 and Fig. 9. In the same figures it can be observed that the transition zone from the soft to the hard solution is always situated within one finite element, an indication of mesh dependency. Changing the element size does not modify the transition from the soft to the hard zone, as no penalization on strain gradient is accounted for in the model.

3.2. Linear perturbation analysis

Various researchers have performed stability analyses looking at the impossibility of using a tangent stiffness operator for the overstress viscoplastic models, see for example [60, 61]. In the following, a different approach is considered, based on the notion of stability defined by Lyapunov [62] that states that a configuration is stable when any perturbation remains close to it or asymptotically extinguishes. Stability is thus directly connected with the time evolution of a system, see also [40].

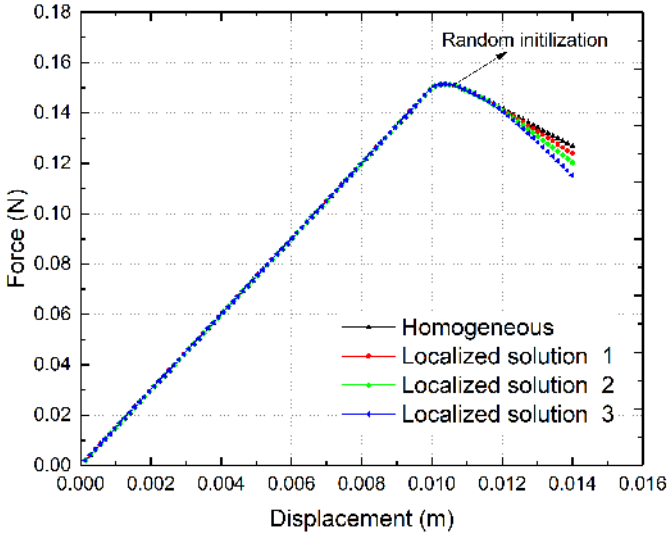

Figure 7: Global responses: localized solutions obtained with random initialization (classical medium)

(a) Localized solution 1 (b) Localized solution 2 (c) Localized solution 3

Figure 8: Local responses: localized solutions, distribution of the accumulated equivalent plastic strain along the length of the bar obtained using random initialization, peak point (Cauchy medium)

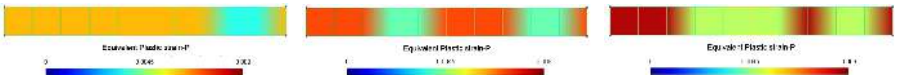

(a) Localized solution 1 (b) Localized solution 2 (c) Localized solution 3

Figure 9: Local responses: localized solutions, distribution of the accumulated equivalent plastic strain along the length of the bar obtained using random initialization, last step (Cauchy medium)

Let's consider now a periodic perturbation in the displacement δu imposed on the homogeneous solution $\hat{u}$ such that

$$\delta u = \hat{u} e^{\omega t + ikx} \tag{46}$$

with k the wave number, ω the growth rate and $\hat{u}$ the amplitude, of order $\hat{u} \ll 1$. We get:

$$\begin{aligned} \delta\dot{u} &= \frac{\partial \delta u}{\partial t} = \omega \delta u & \delta\gamma &= \frac{\partial \delta u}{\partial x} = ik\delta u \\ \delta\gamma_{,x} &= \frac{\partial \delta\gamma}{\partial x} = -k^2 \delta u & \delta\dot{\gamma} &= \frac{\partial \delta\gamma}{\partial t} = ik\omega\delta u \\ \delta\dot{\gamma}_{,x} &= \frac{\partial \delta\dot{\gamma}}{\partial x} = -k^2\omega\delta u \end{aligned} \tag{47}$$

The perturbation of the viscoplastic strain is obtained as

$$\delta\dot{\gamma}^{vp} = \frac{1}{\eta\sigma_{max}} \left(\delta\sigma - A_2 \delta\gamma\right) \tag{48}$$

Differentiation of the two sides of equation (48) with respect to x yields

$$\delta\dot{\gamma}^{vp}_{,x} = \frac{k^2 A_2}{\eta\sigma_{max}} \delta u \tag{49}$$

where the term $\delta\sigma_{,x} = 0$ vanishes according to equilibrium equation.

Furthermore, the perturbation of the constitutive law (equation (27)) leads to

$$\delta\dot{\gamma}^{vp}_{,x} = -\frac{\delta\dot{\sigma}_{,x}}{A_1} + \delta\dot{\gamma}_{,x} = -k^2\omega\delta u \tag{50}$$

Equating expressions (49) and (50) provides the characteristic stability equation:

$$\omega = -\frac{A_2}{\eta\sigma_{max}} \tag{51}$$

For ω real and positive the perturbation grows with time and the homogeneous solution is unstable. For ω real and negative the perturbed solution decays with time and the homogeneous solution is stable. The following remarks/conclusions can be made:

- η and σ_{max} being positive, the sign of the growth rate depends on the sign of the hardening modulus A_2. As long as A_2 is non-negative, the growth rate decays with time and the behavior is stable. When softening occurs ($A_2 < 0$), the growth rate increases exponentially and the behavior is unstable.
- The growth rate is independent of the wave number k and therefore of the wave length perturbation ($\lambda = 2\pi/k$). Its magnitude is inversely proportional to the viscosity η and the yield stress $\sigma_{\max}$.
- The wave length λ does not control the growth rate of the perturbation. In other words, it is not the size of the finite element that controls localization, as for the case when inertia terms are considered [40]. The behavior being however unstable after the peak, numerical results depend on existing perturbations related for example to material imperfections and loading conditions which might favor one wave length, as mentioned in [40].

4. Two-dimensional numerical study in a Cauchy medium

A biaxial numerical test with an elasto-viscoplastic constitutive law is conducted hereafter to illustrate the loss of uniqueness of the solution and the mesh dependency problems that can arise.

4.1. The MCC viscoplastic model

The consistency viscoplastic model formulation [26] is chosen due to its robust implementation algorithm [63] and its ability to reproduce a smooth transition between rate-dependent and rate-independent solutions [64]. The viscoplastic model is based on the pressure sensitive Modified Cam Clay (MCC) model often used for clayey geomaterials [65]. The well-known yield function of the MCC model is given by:

$$f(\sigma, p_c) = \frac{q^2}{M^2} + p(p - p_c) \tag{52}$$

where p is the mean effective stress, q the deviatoric stress, p_c the preconsolidation pressure (say the maximum pressure ever experienced by the soil sample) and M the slope of the critical state line in the $p - q$ plane (say the locus of those states of the material where shear distortions occur without any further changes in mean effective stress or deviatoric stress or void ratio). An associated flow rule is adopted for simplicity depending on the plastic strain and strain rate:

$$\frac{\partial p_c}{\partial \kappa} = h, \; \frac{\partial p_c}{\partial \dot{\kappa}} = y \tag{53}$$

where h and y are hardening functions associated with the internal variables κ and $\dot{\kappa}$. Following the classical MCC model formulation $\kappa = \varepsilon_v^{vp}$, the volumetric visco-plastic strain and h is given as:

$$h = \nu^* p_c = \frac{1 + e_0}{\lambda^* - \kappa^*} p_c \tag{54}$$

where e_0 denotes the initial void ratio, λ^* the virgin compression index, κ^* the swelling index during a time increment from t_n to t_{n+1} and ν^* the hardening parameter which is considered constant [66].
The hardening function y is assumed constant and equal to the viscosity parameter η:

$$y = \eta \tag{55}$$

The rate form of p_c writes:

$$\dot{p}_c = \nu^* p_c \dot{\kappa} + \eta \ddot{\kappa} \tag{56}$$

The initial preconsolidation pressure p_c and the slope of the critical state line M can be determined from constant strain rate tests, the initial void ratio e_0, the compression index λ^* and the recompression index κ^* from the oedometer test and the viscosity parameter η from three different constant strain rate tests.

4.2. Calibration of the MCC viscoplastic model

The criterion adopted hereafter for the calibration of the viscosity parameter of the MCC viscoplastic model is the ability to reproduce the viscous behavior of a typical clay material. Undrained constant strain rate tests on normally consolidated clays are simulated [67]. The calibrated parameters are presented in Table 2, where the Poisson's ratio ν is taken 0.3, a typical value for soft soils. A good agreement between the experimental and the numerical results is observed in Fig 10, proof of the good calibration of the model. As mentioned in [68], it should however be noticed that the viscosity parameter of the viscoplastic model calibrated from triaxial experiments is typically different from the viscosity parameter measured experimentally using for example fall cone tests or rheometers [69, 70, 71, 72].

Table 2: Calibrated parameters of the MCC viscoplastic model

Category	Parameter	Value
Elastic parameters	Recompression index κ^*	0.06
	Poisson's ratio ν	0.3
Plastic parameters	Compression index λ^*	0.4
	Slope of critical state line M	1.2
Viscous parameter	Viscosity parameter η	$3 \times 10^9 Pa{\cdot}s$
State variables	Initial preconsolidation pressure p_c	$550kPa$
	Initial void ratio e_0	2

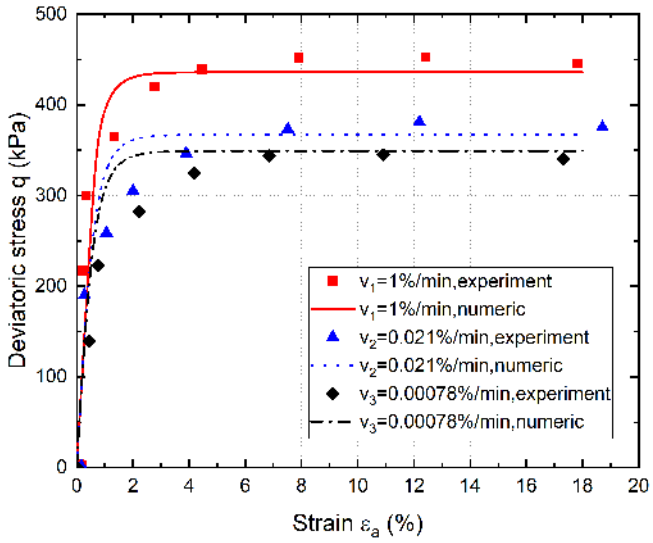

(a) Deviatoric stress versus strain

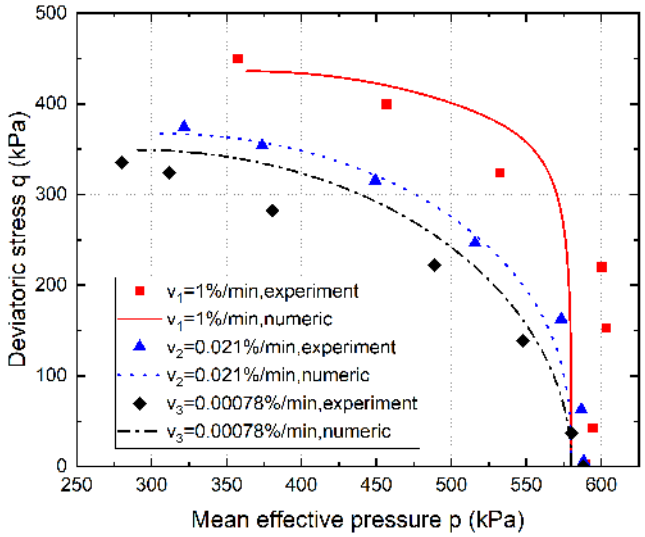

(b) Mean effective stress versus deviatoric stress

Figure 10: Viscoplastic MCC model: comparison between experimental and numerical results

4.3. Biaxial test

The geometry, the applied loading and the boundary conditions of the biaxial plain strain test reproduced numerically with the viscoplastic MCC model are described hereafter. The aspect ratio is taken equal to 2 (height 1m and width 0.5m), small enough to avoid the occurence of buckling before the shear band localization, see Fig 11. The specimen is submitted to a constant lateral confining pressure and to an imposed vertical displacement at the top. At the bottom, all vertical displacements are constrained and the horizontal direction of the middle point is fixed. Perfect sliding is assumed at the top and the bottom of the specimen. The confining pressure is 50 kPa and the preconsolidation pressure 550 kPa, the soil specimen is thus in a state of overconsolidation (OCR=11). Softening occurs therefore for a stress level higher than the critical state. Once the yield surface is attained, plastic deformation makes it shrink.

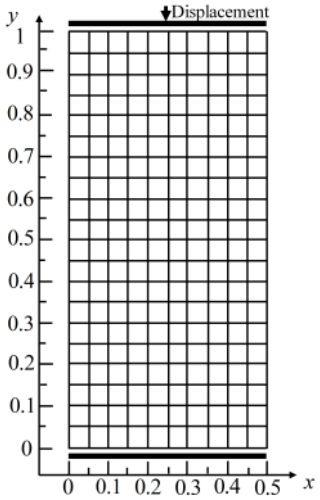

Figure 11: Loading and boundary conditions of the biaxial test

4.3.1. Loss of uniqueness

Three loading rates are considered, 0.002% m/min, 0.02% m/min, 0.2% m/min corresponding to a small, a medium and large loading rate respectively. The global responses are given in Fig 12 where it can be observed that different rates result in different peak points. The peak points are delayed by the rate effects, a result consistent with the 1D analysis presented in section 3.1.

Loss of uniqueness is first studied in terms of the Hill's criterion (equation (4)). It is found that the Hill criterion is no longer satisfied at the peak points of Fig12 for the MMC model with or without rate effects.

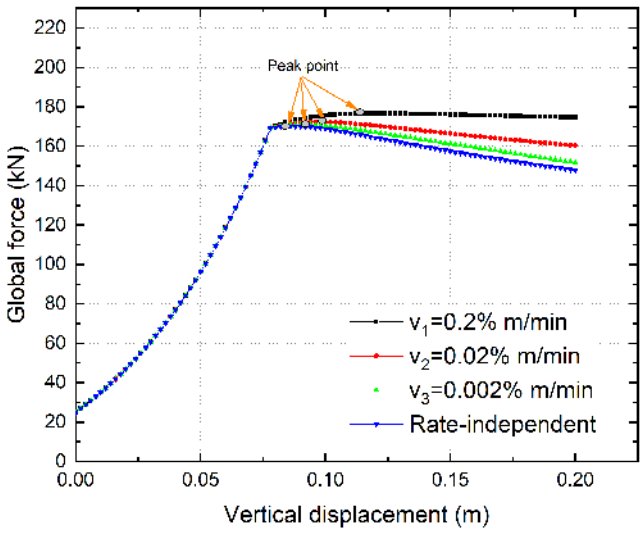

Figure 12: Biaxial test: force-displacement curves for different loading rates (Cauchy medium)

From the peak points on (increasing displacements) the uniqueness of the solution is therefore no longer guaranteed.

Shear band formation in bifurcation points is then investigated by means of the Rice criterion, equation (11), see Fig 13. Four characteristic steps are selected: elastic step, first plastic step, first bifurcated step and last step as shown in Fig 13(a). The evolution of the Rice criterion associated to the uniform solution is presented during the increasing loading history in Fig 13(b) as a function of $\tan\theta$, where θ is the orientation of the shear band normal to the loading vertical axis, i.e. the shear band orientation with the horizontal direction. The determinant of the acoustic tensor $det(Q)$ is calculated using equation (13) and plotted here as a normalized value with respect to a fixed value (the determinant at the first elastic step). It can be seen that for the elastic step, the determinant of the acoustic tensor is always positive. As the loading increases up to the first plastic step, two extrema appear but the minimum value of the determinant remains positive. Later on, a bifurcation point with two possible bifurcated directions occurs, since a double real solution appears. At this point, that coincides with the peak of the global curve, the Hill's criterion is also violated as the flow rule is associated, see also section 3.1.2 and [73]. From higher levels of loading, four possible bifurcated directions occur till the last step. A similar evolution was found for rate independent materials

[74] and for multiphysics couplings [75].

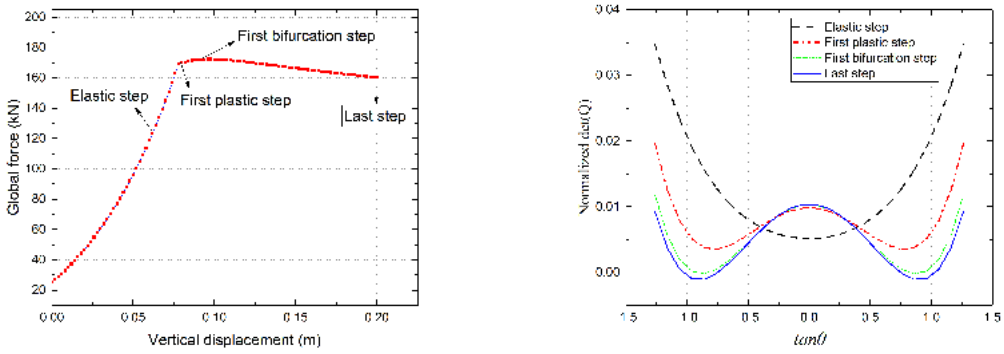

(a) Four characteristic steps

(b) Evolution of the Rice criterion

Figure 13: Biaxial test: evolution of the Rice criterion for four characteristic steps (Cauchy medium)

Another way to illustrate different bifurcated possible solutions is to apply the algorithm for the random initialization, see section 2.3. Fig 14 presents the homogeneous solution, a bifurcated solution and the position of the bifurcation point (after the peak point, corresponding to a vertical displacement of 0.0098 m). At the local level, two modes of strain localization are illustrated in Fig 15.

4.3.2. Mesh dependency

Numerical simulations are presented hereafter to illustrate the mesh dependency that occur when using viscoplastic constitutive laws ($v = 0.02\% \, m/min$). Weak elements are introduced to trigger localization in three different meshes: a coarse mesh of 10×20 elements, a medium mesh of 20×40 and a fine mesh of 30×60 elements. The area of the weak elements is kept the same for three mesh refinements. The global and local responses (last step) for the three meshes under a medium imposed loading rate are given in Fig 16 and Fig 17. It can be observed that the size of the finite element mesh controls the solution at the global level but also the width and the magnitude of the shear bands.

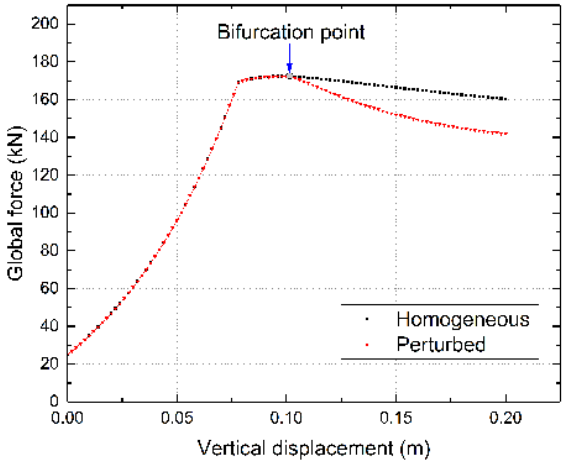

Figure 14: Biaxial test: the homogeneous solution and a bifurcated solution obtained using random initialization (Cauchy medium), ($v = 0.02\% \, m/min$)

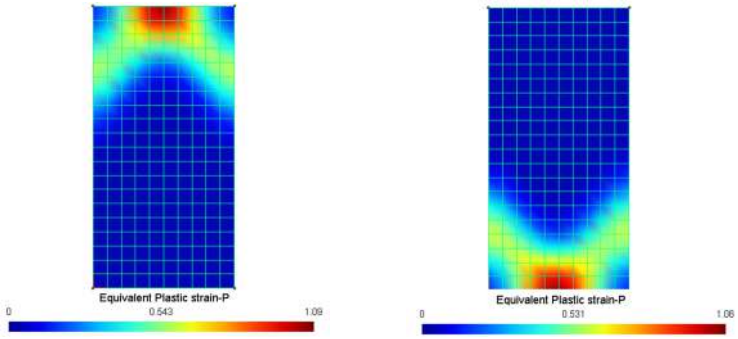

(a) Example 1 (b) Example 2

Figure 15: Biaxial test: two examples of localized solutions obtained using random initialization (Cauchy medium), ($v = 0.02\% \, m/min$)

In the following, viscoplasticity is introduced in a second gradient medium. The idea is to study the behavior within a model that explicitly introduces a material length parameter in order to correctly reproduce strain localization phenomena.

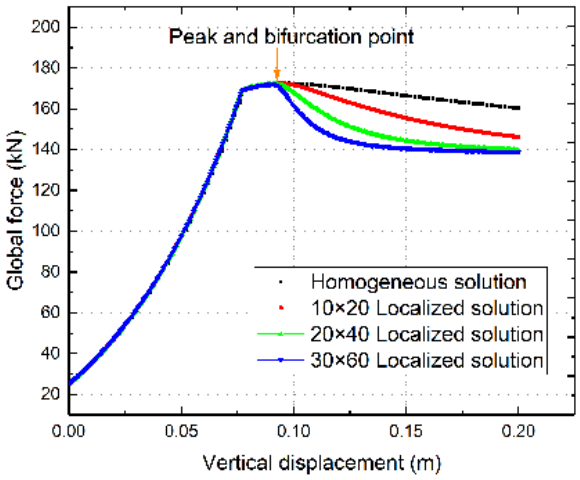

Figure 16: Biaxial test: global response for different mesh sizes (Cauchy medium), ($v = 0.02\% \, m/min$)

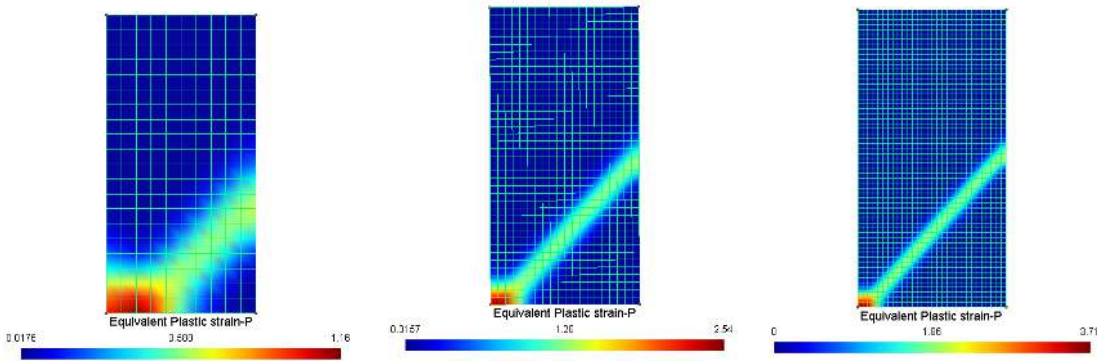

(a) 10×20 elements (b) 20×40 elements (c) 30×60 elements

Figure 17: Biaxial test: distribution of accumulated equivalent plastic strain at the last loading step for different mesh sizes (Cauchy medium), ($v = 0.02\% \, m/min$)

5. One-dimensional analytical and numerical study in a second gradient medium

The second gradient continua belong to the class of continua with microstructure or micromorphic media, see e.g. Germain [9] and Mindlin [10]. While kinematics of a Cauchy continuum is defined by a displacement field, in a a continuum with microstructure an additional field of second order tensors is con-

sidered (called "microkinematic gradient"), which models the strains and the rotation of the microstructure itself (for instance the grains in the case of soils). The virtual work is therefore a linear form with respect to the displacement gradient, the microkinematic gradient and its gradient [10, 76]· In the second gradient model, the microstrain is assumed to be equal to the classical (macro)strain. It has been proven, see e.g. [76, 77, 78], that this model, introducing at least one characteristic length, is capable to regularize boundary value problems and to provide mesh independent results. Moreover it can be easily adapted to every kind of classical constitutive equation (elasto-plastic, damage or hypoplastic), see among others [59, 79, 80, 81, 82].

It is of interest to investigate again stability, say the onset condition for the growth of small periodic perturbations, within this model. Consider again the 1D bar subjected to an axial displacement at the right and fixed at the left end. Lets call also a and b its two extremities, see Fig 3. The 1D problem in a second gradient continuum is briefly recalled hereafter [77]. The internal virtual work is given as

$$W_{in}^{*} = \int_a^b (\sigma \frac{\partial u^*}{\partial x} + \Sigma \frac{\partial^2 u^*}{\partial x^2}) dx \tag{57}$$

with Σ the double stress and * the superscript defining virtual quantities. By means of the virtual work principle and integrating by parts, the balanced equation writes [77]

$$\frac{\partial \sigma}{\partial x} - \frac{\partial^2 \Sigma}{\partial x^2} = 0 \tag{58}$$

In the following, the 1D first gradient constitutive law is the one of Fig 1 and equation (25). A linear elastic relation is assumed for the 1D second gradient constitutive law that takes the following form:

$$\Sigma = D_{sg} \frac{\partial^2 u}{\partial x^2} \tag{59}$$

The first and second gradient constitutive laws are considered uncoupled. The viscoplastic strain rate is again given by equation (26).

5.1. Linear perturbation analysis

The same steps as in section 3.2 are followed hereafter. Starting from the following equations

$$\begin{aligned} \dot{\sigma} &= A_1 \left(\dot{\gamma} - \dot{\gamma}^{vp}\right) \\ \dot{\gamma}^{vp} &= \frac{1}{\eta \sigma_{max}} [\sigma - \sigma_{max} - A_2(\gamma - \gamma_{lim})] \\ \Sigma &= D_{sg} \frac{\partial^2 u}{\partial x^2} \end{aligned} \tag{60}$$

the same displacement perturbation of the homogeneous solution as in equation (46) is considered

$$\delta u = \hat{u} e^{\omega t + ikx} \tag{61}$$

Besides the equations (47), two additional relationships have to be considered

$$\begin{aligned} \delta u_{,xxxx} &= k^4 \delta u \\ \delta \dot{u}_{,xxxx} &= \frac{\partial u_{,xxxx}}{\partial t} = \omega k^4 \delta u \end{aligned} \tag{62}$$

The perturbation of the equilibrium equation (58) gives

$$\delta \sigma_{,x} - D_{sg} \delta u_{,xxxx} = 0 \tag{63}$$

Its rate form gives

$$\delta \dot{\sigma}_{,x} - D_{sg} \delta \dot{u}_{,xxxx} = 0 \tag{64}$$

The next step is to perturb the plastic strain rate given by the second equation in (60). Differentiating both sides of the equation with respect to x gives

$$\delta \dot{\gamma}^{vp}_{,x} = \frac{k^4 D_{sg} + k^2 A_2}{\eta \sigma_{max}} \delta u \tag{65}$$

Differentiating both sides of the first gradient constitutive law (equation (60)) and using equation (64) provides

$$\delta \dot{\gamma}^{vp}_{,x} = -k^2 \omega \delta u - \omega k^4 \frac{D_{sg}}{A_1} \delta u \tag{66}$$

Equating equations (65) and (66) and considering that δu is not zero, the characteristic stability equation finally becomes

$$\omega = -\frac{k^2 D_{sg} + A_2}{\eta \sigma_{max} \left(1 + k^2 \frac{D_{sg}}{A_1}\right)} \tag{67}$$

To further investigate the relation between the growth rate ω, the wave length $\lambda = 2\pi/k$ and the second gradient parameter D_{sg} Fig 18 is plotted considering $A_1 = 150kPa, A_2 = -75kPa, \gamma_{lim} = 0.1, \eta = 5Pa$.

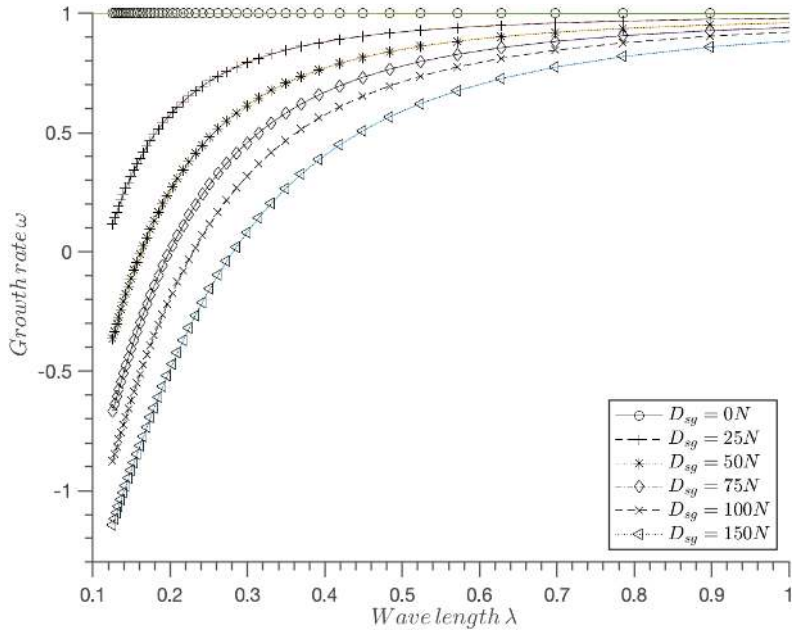

Figure 18: Influence of the wave length λ and the second gradient parameter D_{sg} on the growth rate ω

The following remarks/conclusions can be made:

- When the second gradient parameter D_{sg} vanishes, equation (67) degenerates into equation (51).
- With $D_{sg} \neq 0$, the solution becomes unstable when $-k^2 D_{sg} - A_2 > 0$.
- A critical wave number can be defined as $k_{cr} = \sqrt{\frac{-A_2}{D_{sg}}}$.
- The critical wave length $\lambda_{cr} = 2\pi/k_{cr} = 2\pi\sqrt{\frac{D_{sg}}{-A_2}}$ is equal with the (approximate) internal length of the second gradient medium, see also [77].
- The wave length of the perturbation has to be bigger than the critical wave length for the solution to be unstable and localization to occur (see also [40] and Fig. 18). Otherwise the behavior is stable.
- Increasing the second gradient parameter D_{sg} slows the perturbation growth. The range of the growth rate is limited between $-\frac{A_1}{\eta\sigma_{max}} \leq \omega \leq -\frac{A_2}{\eta\sigma_{max}}$, irrespective of the second gradient parameter D_{sg} and the wave length λ.

Remark: The range of the growth rate is found as follows. Equation (67) is multiplied with the denomi-

nator $\eta\sigma_{max}\left(1+k^2\frac{D_{sg}}{E}\right)$ and after some algebra we arrive at an quadratic equation for k:

$$\left(\omega\eta\sigma_{max}\frac{D_{sg}}{A_1}+D_{sg}\right)k^2+(\omega\eta\sigma_{max}+A_2)=0 \tag{68}$$

In order for at least one solution to exist for k, the discriminant should be equal or larger than 0:

$$\Delta=-4\left(\omega\eta\sigma_{max}\frac{D_{sg}}{A_1}+D_{sg}\right)(\omega\eta\sigma_{max}+A_2)\geqslant 0 \tag{69}$$

6. Two-dimensional numerical study in a second gradient medium

In order to reproduce the two-dimensional plane strain numerical study of section 4 in a second gradient medium, the second gradient finite element formulation introduced in [77, 78, 83] is adopted in the following. The viscoplastic MCC of section 4.1 is considered for the first gradient part (with the material parameters of table 2), ($v=0.02\%\,m/min$). Although the constitutive law for the second gradient part can introduce various material characteristic lengths [84], a simple law is adopted hereafter with the second gradient slope D_{sg} as the only parameter. This simplified second gradient law has been often used in previous works, see for example [78], [80], [82] and [85]. D_{sg} is set equal to $350N$.

Fig 19 presents the results of numerical simulations. It can be seen that they do not depend on the number of finite elements. Furthermore, when a structured mesh as in Fig 20(a), a biased mesh as in Fig 20(b) and a

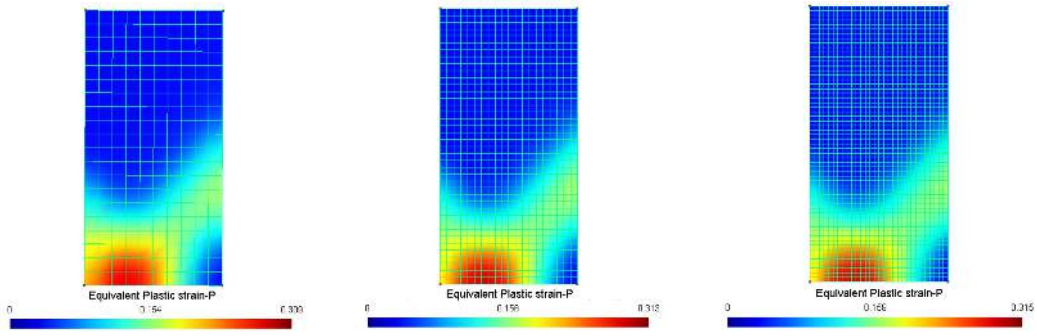

(a) 10×20 elements (b) 20×40 elements (c) 30×60 elements

Figure 19: Biaxial test: distribution of accumulated equivalent plastic strain for different mesh sizes, last loading step, $D_{sg}=350N$ (second gradient medium), ($v=0.02\%\,m/min$)

non-structured mesh as in Fig 20(c) are chosen, results are also found independent on the mesh orientation, Fig 21.

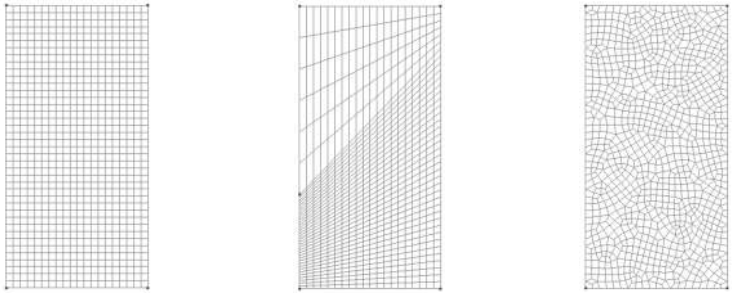

(a) Structured mesh (b) Biased mesh (c) Non structured mesh

Figure 20: Biaxial test: three different types of mesh

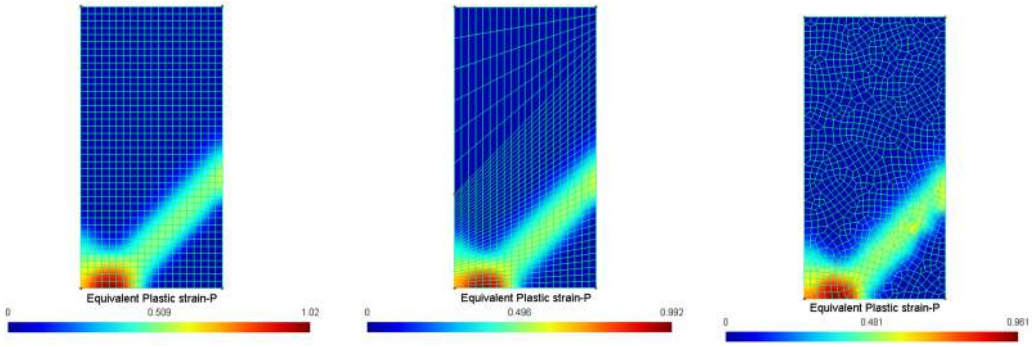

(a) Structured mesh (b) Biased mesh (c) Non structured mesh

Figure 21: Biaxial test: distribution of accumulated equivalent plastic strain for different mesh orientations, last loading step, $D_{sg} = 50N$ (second gradient medium), ($v = 0.02\% \, m/min$)

The effect of the second gradient parameter D_{sg} on the global and local behavior is studied hereafter. Fig 22 and Fig 23 show that the width of shear band is governed by the chosen D_{sg}. The larger the value of D_{sg} the smoother the slope of the post-peak global response and the bigger the shear band width. A parametric study is finally performed to find qualitatively the relation between the second gradient parameter and the shear band width. Similar to the 1D case, the shear band thickness is found proportional to the square root of the second gradient parameter, see Fig 24. This relation can be used as a first estimate to calibrate the second gradient parameter for the desired shear band width.

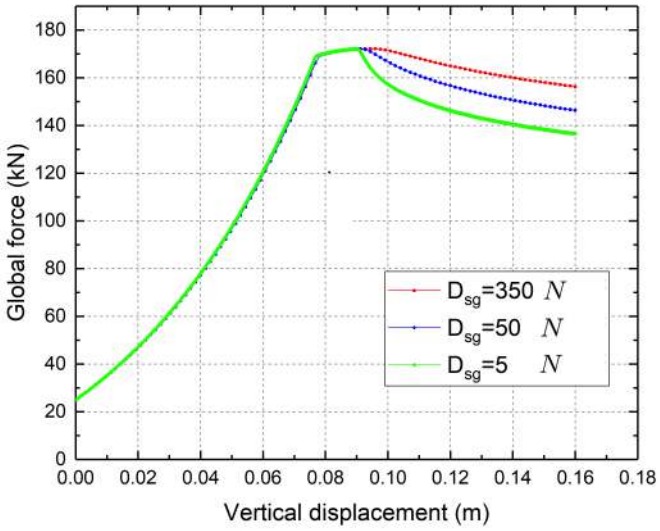

Figure 22: Biaxial test: force-displacement curves for different second gradient parameters, ($v = 0.02\% \, m/min$)

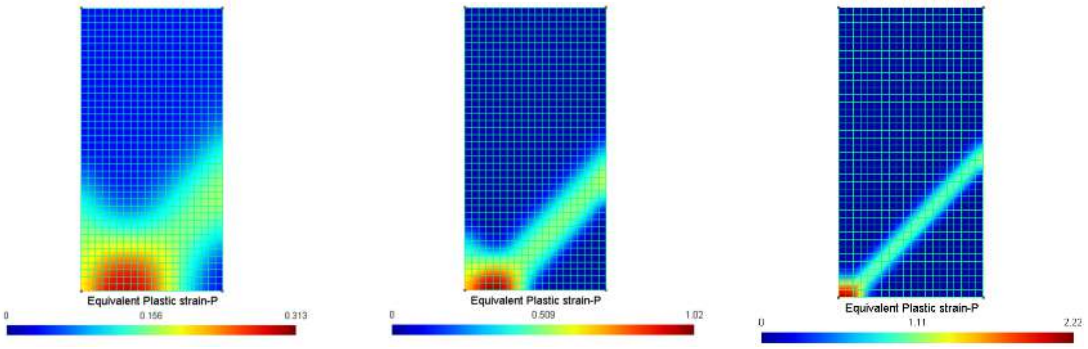

(a) $D_{sg} = 350N$ (b) $D_{sg} = 50N$ (c) $D_{sg} = 5N$

Figure 23: Biaxial test: distribution of accumulated equivalent plastic strain for different second gradient parameters, last loading step, ($v = 0.02\% \, m/min$)

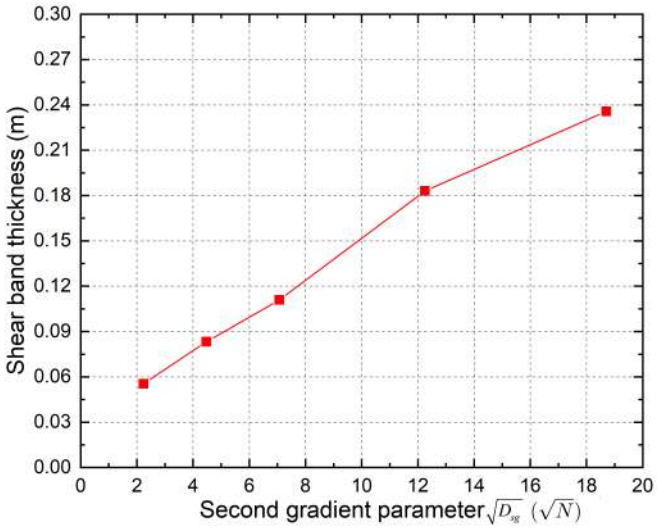

Figure 24: Biaxial test: relationship between the square root of the second gradient parameter and the shear band thickness

305 Finally, the effect of the viscosity parameter in a second gradient continuum is illustrated in Fig 25 and Fig 26. Overall, for a given second gradient parameter ($D_{sg} = 350N$), it is observed that a higher viscosity leads to a more ductile post-peak response and an increase of the shear band thickness. Fig 25 and Fig 26 also depict that a high viscosity results in a significant delay in the development of equivalent plastic strain

and thus a decrease of maximum accumulated equivalent plastic strain.

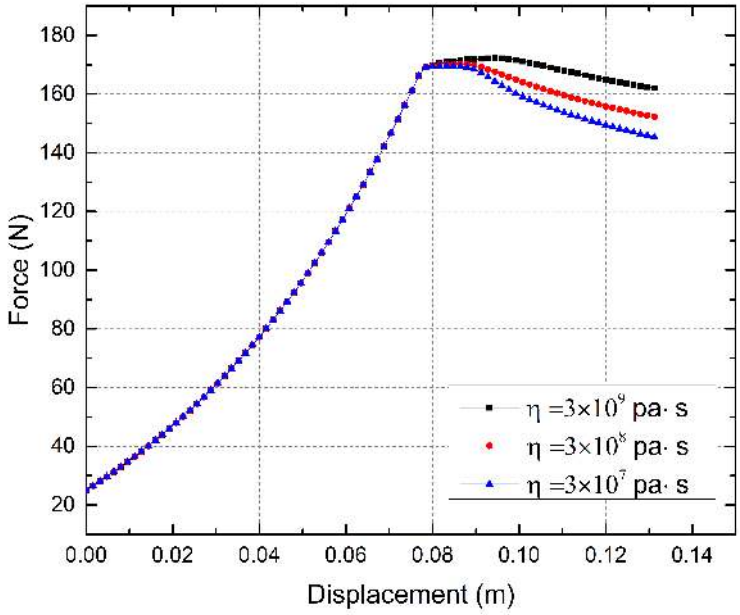

Figure 25: Biaxial test: force-displacement curves for different viscosities in a second gradient medium ($D_{sg} = 350N$)

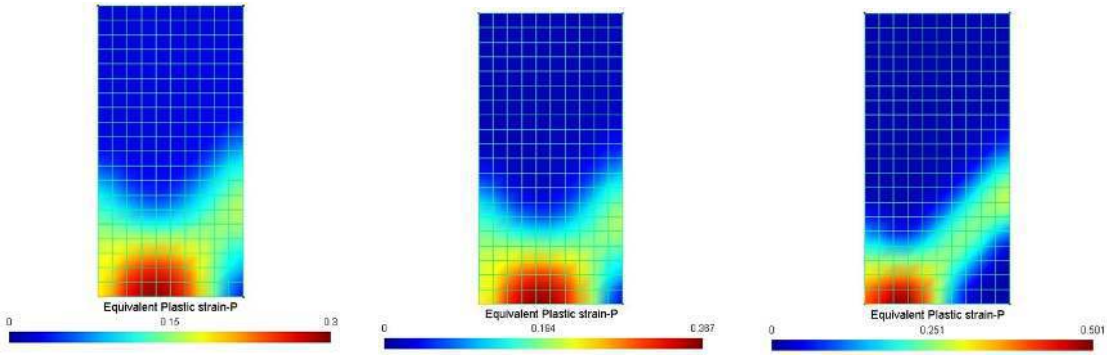

(a) $\eta = 3X10^9\, pa.s$ (b) $\eta = 3X10^8\, pa.s$ (c) $\eta = 3X10^7\, pa.s$

Figure 26: Biaxial test: distribution of accumulated equivalent plastic strain at the last loading step for different viscosities in a second gradient medium ($D_{sg} = 350N$)

7. Conclusions

Non-uniqueness, stability and bifurcation analyses were presented for elasto-viscoplastic boundary value problems in a Cauchy and a second gradient medium. All inertia forces were neglected. The main findings are summarized hereafter.

In a Cauchy medium, elasto-viscoplasticity does not restore the uniqueness of the solution. As no internal length is introduced, the number of possible solutions is infinite and the results can be therefore erroneous. Viscoplasticity introduces also a critical time and delays the occurrence of instabilities by increasing the hardening part of the constitutive law and therefore inducing a structural hardening. The 1D linear perturbation analysis shows that the wave length does not control the growth rate of the perturbation. The behavior being however unstable after the peak, numerical results depend on existing perturbations.

In a second gradient medium, elasto-viscoplasticity does not restore the uniqueness of the solution. Nevertheless, as an internal length is introduced, the number of possible solutions is finite and the results are objective (independent on the number and orientation of the finite elements). Rate dependent behaviors can be correctly reproduced coupling viscoplasticity and second gradient continua. The 1D linear perturbation analysis shows that the wave length of the perturbation has to be bigger than a critical wave length for the solution to be unstable and localization to occur.

It would be interesting to further study the relationship between the different approaches to the problem with regard to the Theory of Controllability proposed by Nova and co-workers - a summary of the main results is given in [86].

In the literature, viscoplasticity is sometimes proposed to regularize quasi-static boundary value problems. It is the authors opinion that when the aim is to reproduce a rate-independent behavior, a high value of viscosity can sometimes provide mesh independent results, up to a certain limit of deformations, because it actually modifies the response of the constitutive law by an ad-hoc increase of its hardening part. One should however question if such modification of the constitutive law reproduces the realistic rate-independent behavior of the material. Furthermore, it is difficult to know a priori the adequate viscosity value to adopt under 3D complex loadings. When on the other hand the aim is to reproduce the rate dependent behavior, the viscosity parameter should be calibrated by triaxial tests. This of course limits the acceptable values of the viscosity parameter and therefore mesh dependency often occurs. For example, while some success, at least in dynamic problems, could be scored for the case of clayey geomaterials which are strongly viscous, purely viscous regularisation for sands would be unsuccessful given how weakly viscous they are (especially dense sand, see [87]).

It is therefore advisable and much more versatile to combine viscoplasticity with a method that introduces a length scale in boundary value problems (e.g. higher order continua or non local models), the role of viscosity being limited to reproduce rate phenomena and the role of the internal length parameter to regularize the results.

8. Acknowledgments

We thank the China Scholarship Council (CSC) for funding the doctoral fellowship of the first author.

Appendix A. Perzyna, Duvaut-Lions and Consistent models: 1D viscoplastic strain rates

The 1D viscoplastic formulation is given hereafter following the Perzyna, the Duvaut-Lions and the Consistent model. It is shown that under certain conditions the 1D viscoplastic strain rate formulations of the three models are identical (see also [25]).

Perzyna model

The viscoplastic strain rate in Perzyna model [12, 13] is given as:

$$\dot{\gamma}^{vp} = \frac{1}{\eta} < \Phi(f) > \frac{\partial g}{\partial \sigma} \tag{A.1}$$

where η is the viscosity parameter, g the potential function and $\Phi(f)$ the overstress function. The symbol $< \cdot >$ indicates the McCauley brackets, defined as:

$$\langle \Phi(f) \rangle = \begin{cases} 0 & (\Phi(f) \leqslant 0) \\ \Phi(f) & (\Phi(f) > 0) \end{cases} \tag{A.2}$$

If the overstress function $\Phi(f)$ is chosen as $\Phi(f) = \frac{f}{\sigma_{max}}$, with $f = g$ the rate independent yield function given by equation (25), substitution of $\Phi(f)$ in equation (A.1) provides the 1D viscoplastic strain rate:

$$\dot{\gamma}^{vp} = \frac{1}{\eta \sigma_{max}} [\sigma - \sigma_{max} - A_2(\gamma - \gamma_{lim})] \tag{A.3}$$

Duvaut-Lions overstress model

In the Duvaut-Lions overstress model [14], the viscoplastic strain rate is determined by the difference between the states associated to the rate-dependent and the rate-independent solutions:

$$\dot{\gamma}^{vp} = \frac{\boldsymbol{A}^{-1}}{\eta} (\sigma - \sigma_{\infty}) \tag{A.4}$$

where as before η is the viscosity, σ is the stress state associated to the rate-dependent solution and σ_∞ the stress state associated to the rate-independent solution. The fourth-order tensor $\boldsymbol{A}$ defines the projection of the difference between the two stress states; two particular cases of $\boldsymbol{A}$ are the unit fourth-order tensor $\boldsymbol{I}_{ijkl}$ [14] and the elastic moduli $\boldsymbol{C}_{ijkl}$ [15].

In this model, the viscoplastic strain rate (equation (A.4)) depends on σ_∞. Adopting a bilinear 1D constitutive law, as in Fig 1, σ_∞ is found equal to:

$$\sigma_\infty = \sigma_{max} + A_2(\gamma - \gamma_{lim}) \tag{A.5}$$

The 1D viscoplastic strain rate becomes therefore:

$$\dot{\gamma}^{vp} = \frac{1}{\eta A}[\sigma - \sigma_{max} - A_2(\gamma - \gamma_{lim})] \tag{A.6}$$

It is obvious that the 1D viscoplastic strain rate of the Duvaut-Lions model coincides with the 1D Perzyna's viscoplastic rate if:

$$A = \sigma_{max} \tag{A.7}$$

Consistent viscoplastic model

The yield function of the Consistent viscoplastic model depends on the strain and the strain rate. For the 1D case (see Fig 1) one gets:

$$f(\sigma, \gamma, \dot{\gamma}) = \sigma - \sigma_{max} - \gamma^{vp}\frac{A_1 A_2}{A_2 - A_1} - y\dot{\gamma}^{vp} \tag{A.8}$$

where y is the hardening function related to the strain rate effect. In order to get the same expression as for the two overstress models, y can be chosen as [38]:

$$y = \eta\left(\frac{d\Phi\left(f\right)}{df}\right)^{-1} = \eta\sigma_{max} \tag{A.9}$$

The 1D strain rate formulations of the three viscoplastic laws coincide therefore if $\Phi(f) = \frac{f}{\sigma_{max}}$, $A = \sigma_{max}$ and $y = \eta\sigma_{max}$.

References

[1] E. C. Aifantis, On the microstructural origin of certain inelastic models, Journal of Engineering Materials and technology 106 (4) (1984) 326–330.

[2] Z. P. Bazant, G. Pijaudier-Cabot, Nonlocal continuum damage, localization instability and convergence, Journal of applied mechanics 55 (2) (1988) 287–293.

[3] I. Vardoulakis, E. Aifantis, A gradient flow theory of plasticity for granular materials, Acta mechanica 87 (3) (1991) 197–217.

[4] I. Vardoulakis, G. Frantziskonis, Micro-structure in kinematic-hardening plasticity, European Journal of Mechanics, A/Solids 11 (4) (1992) 467–486.

[5] R. De Borst, H.-B. Mühlhaus, Gradient-dependent plasticity: formulation and algorithmic aspects, International Journal for Numerical Methods in Engineering 35 (3) (1992) 521–539.

[6] J. Sulem, I. Vardoulakis, Bifurcation analysis in geomechanics, CRC Press, 1995.

[7] M. Fréemond, B. Nedjar, Damage, gradient of damage and principle of virtual work, Internat. J. Solids Struct 33 (1996) 1083–1103.

[8] P. Germain, La méthode des puissances virtuelles en mécanique des milieux continus, premiere partie: théorie du second gradient, J. Mécanique 12 (2) (1973) 235–274.

[9] P. Germain, The method of virtual power in continuum mechanics. part 2: Microstructure, SIAM Journal on Applied Mathematics 25 (3) (1973) 556–575.

[10] R. D. Mindlin, Micro-structure in linear elasticity, Archive for Rational Mechanics and Analysis 16 (1) (1964) 51–78.

[11] R. D. Mindlin, Second gradient of strain and surface-tension in linear elasticity, International Journal of Solids and Structures 1 (4) (1965) 417–438.

[12] P. Perzyna, The constitutive equations for rate sensitive plastic materials, Quarterly of applied mathematics 20 (4) (1963) 321–332.

[13] P. Perzyna, Fundamental problems in viscoplasticity, Advances in applied mechanics 9 (1966) 243–377.

[14] G. Duvaut, J. L. Lions, Les inéquations en mécanique et en physique, Travaux Recherches Math., Dunod, Paris, 1972.
URL http://cds.cern.ch/record/212412

[15] J. Simo, J. Kennedy, S. Govindjee, Non-smooth multisurface plasticity and viscoplasticity. loading/unloading conditions and numerical algorithms, International Journal for Numerical Methods in Engineering 26 (10) (1988) 2161–2185.

[16] P. M. Naghdi, A critical review of the state of finite plasticity, Zeitschrift für angewandte Mathematik und Physik ZAMP 41 (3) (1990) 315–394.

[17] M. Rubin, O. Vorobiev, L. Glenn, Mechanical and numerical modeling of a porous elastic–viscoplastic material with tensile failure, International Journal of Solids and Structures 37 (13) (2000) 1841–1871.

[18] L. Anand, K. Kim, T. Shawki, Onset of shear localization in viscoplastic solids, Journal of the Mechanics and Physics of Solids 35 (4) (1987) 407–429.

[19] J. Pan, Perturbation analysis of shear strain localization in rate sensitive materials, International Journal of Solids and Structures 19 (2) (1983) 153–164.

[20] I. Dobovsek, B. Moran, Material instabilities in rate dependent solids, European journal of mechanics. A. Solids 15 (2) (1996) 267–294.

[21] A. Needleman, Material rate dependence and mesh sensitivity in localization problems, Computer methods in applied mechanics and engineering 67 (1) (1988) 69–85.

[22] W. Wang, L. Sluys, Formulation of an implicit algorithm for finite deformation viscoplasticity, International Journal of Solids and Structures 37 (48-50) (2000) 7329–7348.

[23] L. Sluys, R. De Borst, Wave propagation and localization in a rate-dependent cracked medium—model formulation and one-dimensional examples, International Journal of Solids and Structures 29 (23) (1992) 2945–2958.

[24] R. de Borst, T. Duretz, On viscoplastic regularisation of strain-softening rocks and soils, International Journal for Numerical and Analytical Methods in Geomechanics 44 (6) (2020) 890–903.

[25] W. M. Wang, Stationary and propagative instabilities in metals-a computational point of view, Ph.D. thesis, Delft University of Technology (1997).

[26] W. Wang, L. Sluys, R. De Borst, Viscoplasticity for instabilities due to strain softening and strain-rate softening, International Journal for Numerical Methods in Engineering 40 (20) (1997) 3839–3864.

[27] Y. Leroy, M. Ortiz, Finite element analysis of transient strain localization phenomena in frictional solids, International Journal for Numerical and Analytical Methods in Geomechanics 14 (2) (1990) 93–124.

[28] W. Wang, L. Sluys, R. De Borst, Interaction between material length scale and imperfection size for localisation phenomena in viscoplastic media, Eur. J. Mech., A/Solids 15 (3) (1996) 447–464.

[29] H. Ziegler, C. Wehrli, The derivation of constitutive relations from the free energy and the dissipation function, Vol. 25 of Advances in Applied Mechanics, Elsevier, 1987, pp. 183–238.

[30] J. Lemaitre, J.-L. Chaboche, Mechanics of solid materials, Cambridge university press, 1994.

[31] J.-L. Chaboche, Thermodynamic formulation of constitutive equations and application to the viscoplasticity and viscoelasticity of metals and polymers, International Journal of Solids and Structures 34 (18) (1997) 2239–2254.

[32] G. Houlsby, A. Puzrin, An approach to plasticity based on generalised thermodynamics, in: Constitutive Modelling of Granular Materials, Springer, 2000, pp. 319–331.

[33] R. I. Borja, Cam-Clay plasticity. Part V: A mathematical framework for three-phase deformation and strain localization analyses of partially saturated porous media, Computer Methods in Applied Mechanics and Engineering 193 (48-51) (2004) 5301–5338.

[34] K. R. Rajagopal, A. R. Srinivasa, On the thermomechanics of materials that have multiple natural configurations part i: Viscoelasticity and classical plasticity, Zeitschrift für angewandte Mathematik und Physik ZAMP 55 (5) (2004) 861–893.

[35] H. Ziegler, An introduction to thermomechanics, Elsevier, 2012.

[36] M. Ristinmaa, N. S. Ottosen, Viscoplasticity based on an additive split of the conjugated forces, European Journal of Mechanics-A/Solids 17 (2) (1998) 207–235.

[37] M. Ristinmaa, N. S. Ottosen, Consequences of dynamic yield surface in viscoplasticity, International Journal of Solids and Structures 37 (33) (2000) 4601–4622.

[38] O. M. Heeres, A. S. Suiker, R. de Borst, A comparison between the perzyna viscoplastic model and the consistency viscoplastic model, European Journal of Mechanics-A/Solids 21 (1) (2002) 1–12.

[39] B. Loret, J. H. Prevost, Dynamic strain localization in elasto-(visco-) plastic solids, part 1. general formulation and one-dimensional examples, Computer Methods in Applied Mechanics and Engineering 83 (3) (1990) 247–273.

[40] I. Stefanou, E. Gerolymatou, Strain localization in geomaterials and regularization: rate-dependency, higher order continuum theories and multi-physics, ALERT Doctoral School (2019) 47–85.

[41] A. Stathas, I. Stefanou, The role of viscous regularization in dynamical problems, strain localization and mesh dependency (2021). arXiv:2102.10161.

[42] G. Ljustina, M. Fagerström, R. Larsson, Rate sensitive continuum damage models and mesh dependence in finite element analyses, The Scientific World Journal 2014 (2014).

[43] R. Larsson, S. Razanica, B. L. Josefson, Mesh objective continuum damage models for ductile fracture, International Journal for Numerical Methods in Engineering 106 (10) (2016) 840–860.

[44] P. Pirali, G. H. Liaghat, M. Ahmadi, Viscoplasticity coupled with nonlocalized damage for incompatibilities due to strain softening, Mechanics 86 (6) (2010) 17–23.

[45] C. Di Prisco, S. Imposimato, E. Aifantis, A visco-plastic constitutive model for granular soils modified according to non-local and gradient approaches, International journal for numerical and analytical methods in geomechanics 26 (2) (2002) 121–138.

[46] d. M. Bonnet, A. Frangi, Analyse des solides déformables par la méthode des éléments finis, Les Editions de l'Ecole Polytechnique, 2006.

[47] C. Geuzaine, J.-F. Remacle, Gmsh: A 3-d finite element mesh generator with built-in pre-and post-processing facilities, International journal for numerical methods in engineering 79 (11) (2009) 1309–1331.

[48] R. Hill, A general theory of uniqueness and stability in elastic-plastic solids, Journal of the Mechanics and Physics of Solids 6 (3) (1958) 236–249.

[49] D. Bigoni, Nonlinear solid mechanics: bifurcation theory and material instability, Cambridge University Press, 2012.

[50] D. Bigoni, D. Zaccaria, Loss of strong ellipticity in non-associative elastoplasticity, Journal of the Mechanics and Physics of Solids 40 (6) (1992) 1313–1331.

[51] J. W. Rudnicki, J. Rice, Conditions for the localization of deformation in pressure-sensitive dilatant materials, Journal of the Mechanics and Physics of Solids 23 (6) (1975) 371–394.

[52] M. Ortiz, Y. Leroy, A. Needleman, A finite element method for localized failure analysis, Computer methods in applied mechanics and engineering 61 (2) (1987) 189–214.

[53] R. De Borst, Computation of post-bifurcation and post-failure behavior of strain-softening solids, Computers & Structures 25 (2) (1987) 211–224.

[54] R. Chambon, S. Crochepeyre, R. Charlier, An algorithm and a method to search bifurcation points in non-linear problems, International Journal for Numerical Methods in Engineering 51 (3) (2001) 315–332.

[55] R. De Borst, Non-linear analysis of frictional materials, Ph.D. thesis, TU Delft, Delft University of Technology (1986).

[56] W. Wagner, P. Wriggers, A simple method for the calculation of postcritical branches, Engineering computations 5 (2) (1988) 103–109.

[57] M. Crisfield, J. Wills, Solution strategies and softening materials, Computer methods in applied mechanics and engineering 66 (3) (1988) 267–289.

[58] R. de Borst, Numerical modelling of bifurcation and localisation in cohesive-frictional materials, pure and applied geophysics 137 (4) (1991) 367–390.

[59] P. Kotronis, S. Al Holo, P. Bésuelle, R. Chambon, Shear softening and localization: Modelling the evolution of the width of the shear zone, Acta Geotechnica 3 (2) (2008) 85–97.

[60] F. Pisanò, C. d. Prisco, A stability criterion for elasto-viscoplastic constitutive relationships, International Journal for Numerical and Analytical Methods in Geomechanics 40 (1) (2016) 141–156.

[61] F. Marinelli, F. Pisanò, C. Di Prisco, G. Buscarnera, Model-based interpretation of undrained creep instability in loose sands, Géotechnique 68 (6) (2018) 504–517.

[62] A. M. Lyapunov, The general problem of the stability of motion, International Journal of Control 55 (3) (1992) 531–534.

[63] T. J. Hughes, R. L. Taylor, Unconditionally stable algorithms for quasi-static elasto/visco-plastic finite element analysis, Computers & Structures 8 (2) (1978) 169–173.

[64] N. Mac, B. Shahbodaghkhan, N. Khalili, A constitutive model for time-dependent behavior of clay, World Academy of Science, Engineering and Technology, International Journal of Civil, Environmental, Structural, Construction and Architectural Engineering 8 (6) (2014) 596–601.

[65] K. Roscoe, Mechanical behaviour of an idealized wet clay, in: Proc. 3rd Eur. Conf. Soil Mech. Wiesbaden, 1963, Vol. 1, 1963, pp. 47–54.

[66] R. I. Borja, S. R. Lee, Cam-clay plasticity, part 1: implicit integration of elasto-plastic constitutive relations, Computer Methods in Applied Mechanics and Engineering 78 (1) (1990) 49–72.

[67] T. Adachi, Descriptive accuracy of several existing constitutive models for normally consolidated clays, Proc. T5th ICONMG, 1985 1 (1985) 259–269.

[68] H. Wang, Viscous and second gradient regularization techniques for the description of the behavior of geomaterials, Ph.D. thesis, Ecole Centrale de Nantes (2019).
URL https://tel.archives-ouvertes.fr/tel-02954012

[69] L. E. Vallejo, V. A. Scovazzo, Determination of the shear strength parameters associated with mudflows, Soils and foundations 43 (2) (2003) 129–133.

[70] S. P. Mahajan, M. Budhu, Viscous effects on penetrating shafts in clays, Acta Geotechnica 1 (3) (2006) 157.

[71] S. Mahajan, M. Budhu, Shear viscosity of clays to compute viscous resistance, in: Proceedings of the 12th International Conference of International Association for Computer Methods and Advances in Geomechanics (IACMAG), Goa, India, 2008, pp. 1516–1523.

[72] T. A. Ghezzehei, D. Or, Rheological properties of wet soils and clays under steady and oscillatory stresses, Soil Science Society of America Journal 65 (3) (2001) 624–637.

[73] D. Bigoni, T. Hueckel, Uniqueness and localization—i. associative and non-associative elastoplasticity, International Journal of Solids and structures 28 (2) (1991) 197–213.

[74] F. Collin, S. Levasseur, R. Chambon, Numerical post failure methods in multiphysical problems, European Journal of Environmental and Civil Engineering 13 (7-8) (2009) 983–1004.

[75] F. Collin, P. Kotronis, B. Pardoen, Numerical modelling of multiphysics couplings and strain localization, in: Modelling of instabilities and bifurcation in Geomechnics, Alert Geomaterials, 2016, pp. 247–291, http://alertgeomaterials.eu/publications.

[76] R. Chambon, D. Caillerie, T. Matsuchima, Plastic continuum with microstructure, local second gradient theories for geomaterials: localization studies, International Journal of Solids and Structures 38 (46-47) (2001) 8503–8527.

[77] R. Chambon, D. Caillerie, N. El Hassan, One-dimensional localisation studied with a second grade model, European Journal of Mechanics-A/Solids 17 (4) (1998) 637–656.

[78] T. Matsushima, R. Chambon, D. Caillerie, Large strain finite element analysis of a local second gradient model: application to localization, International journal for numerical methods in engineering 54 (4) (2002) 499–521.

[79] R. Chambon, D. Caillerie, C. Tamagnini, A strain space gradient plasticity theory for finite strain, Computer Methods in Applied Mechanics and Engineering 193 (27-29) (2004) 2797–2826.

[80] P. Bésuelle, R. Chambon, F. Collin, Switching deformation modes in post-localization solutions with a quasibrittle material, Journal of Mechanics of materials and structures 1 (7) (2006) 1115–1134.

[81] B. Pardoen, S. Levasseur, F. Collin, Using local second gradient model and shear strain localisation to model the excavation damaged zone in unsaturated claystone, Rock Mechanics and Rock Engineering 48 (2) (2015) 691–714.

[82] F. Collin, R. Chambon, R. Charlier, A finite element method for poro mechanical modelling of geotechnical problems using local second gradient models, International journal for numerical methods in engineering 65 (11) (2006) 1749–1772.

[83] P. Bésuelle, Implémentation d'un nouveau type d'élément fini dans le code lagamine pour une classe de lois à longueur interne, internal report, FNRS, Belgique, pages 1–17 (2003).

[84] G. Sciarra, S. Vidoli, Asymptotic fracture modes in strain-gradient elasticity: Size effects and characteristic lengths for isotropic materials, Journal of Elasticity 113 (1) (2013) 27–53.

[85] M. Soufflet, G. Jouan, P. Kotronis, F. Collin, Using a penalty term to deal with spurious oscillations in second gradient finite elements, International Journal of Damage Mechanics 28 (3) (2019) 346–366.

[86] G. Buscarnera, G. Dattola, C. di Prisco, Controllability, uniqueness and existence of the incremental response: A mathematical criterion for elastoplastic constitutive laws, International Journal of Solids and Structures 48 (13) (2011) 1867–1878.

[87] M. Lazari, L. Sanavia, C. di Prisco, F. Pisanò, Predictive potential of perzyna viscoplastic modelling for granular geomaterials, International Journal for Numerical and Analytical Methods in Geomechanics 43 (2) (2019) 544–567.